Journal of Materials Chemistry

Cite this: *J. Mater. Chem.*, 2011, **21**, 11760

www.rsc.org/materials

PAPER

Multicolor graphene nanoribbon/semiconductor nanowire heterojunction light-emitting diodes†

Yu Ye,[a] Lin Gan,[b] Lun Dai,*[a] Hu Meng,[a] Feng Wei,[a] Yu Dai,[a] Zujin Shi,[b] Bin Yu,[a] Xuefeng Guo[b] and Guogang Qin*[a]

Received 6th April 2011, Accepted 17th May 2011
DOI: 10.1039/c1jm11441g

We report novel graphene nanoribbon (GNR)/semiconductor nanowire (SNW) heterojunction light-emitting diodes (LEDs) for the first time. In the device, the GNR and SNW have face-to-face contact with each other, which has the merits of a larger active region and smaller series resistance, and may benefit high-efficiency electroluminescence and even electrically driven lasers in the future. ZnO, CdS, and CdSe NWs were employed in our case. At forward biases, the GNR/SNW heterjunction LEDs could emit light with wavelengths varying from ultraviolet (380 nm) to green (513 nm) to red (705 nm), which were determined by the band-gaps of the involved SNWs. The mechanism of light emitting for the GNR/SNW heterojunction LEDs was discussed. Our work opens new routes to developing diverse graphene-based nano-optoelectronic devices, which are basic components in integrated optoelectronic system. Besides, the novel graphene/SNW hybrid devices, by taking advantage of both graphene and SNW, will be promising candidates for use in applications such as high-sensitivity sensor and transparent flexible devices in the future.

Introduction

Graphene, a single atomic layer of carbon arranged in a honeycomb lattice, has attracted a lot of research interest since its discovery in 2004.[1–5] Its many important physical properties, such as high mobility and conductivity,[6] high optical transparency,[7] mechanical flexibility[8] and robustness,[9] environmental stability,[9] and low-temperature processing, have made graphene a promising material for use in diverse device applications. For example, it has been used as a substitute for indium titanium oxide (ITO), which has the drawbacks of high-cost, limited use for flexible substrates, and degradation of device performance over time due to indium diffusion, as the flexible transparent conductive electrode for organic photovoltaics[10] and light-emitting diodes (LEDs).[11] Moreover, graphene is considered a promising alternative to silicon for next-generation nanoelectronics, especially in producing low-cost, high-efficiency, lightweight, transparent, and flexible devices.[5,12–16] So far, although a lot of work has been done on investigating graphene-based electronic devices, little work aimed at developing graphene-based nano-optoelectronic devices, which are basic components in integratred optoelectronic system, has been reported.[17]

Semiconductor single crystalline nanowires (NWs) can be grown and constructed into devices using the bottom-up method[18] on basically any substrate. Moreover, they are mechanically flexible and robust, and are compatible with the low-temperature device process desired for plastic substrates.[19] So far, single NW devices have shown themselves to be promising in high-sensitivity sensors[20] and transparent flexible devices.[19]

In this paper, we report, for the first time, graphene nanoribbon (GNR)/semiconductor NW (SNW) heterojunction LEDs. n-Type ZnO, CdS, CdSe NWs were used in this work. A GNR and SNW face-to-face contact device structure was employed, which has the merits of smaller series resistance and larger active region, and may benefit high-efficiency electroluminescence (EL) and even electrically driven lasers in the future.[21] The emitting light wavelength was determined by the involved SNW. Our work opens new routes to developing diverse graphene-based nano-optoelectronic devices, which are basic components in integrated optoelectronic system. Besides, the novel graphene/SNW hybrid devices, which take advantage of both graphene and SNWs, are promising candidates for use in applications such as high-sensitivity sensor and transparent flexible devices in the future.

Experimental section

Both the n-type SNWs[22–24] and the graphene[25] used in this work were synthesized *via* the CVD method. Before device fabrication,

[a]*State Key Lab for Mesoscopic Physics and School of Physics, Peking University, Beijing, 100871, China. E-mail: lundai@pku.edu.cn; qingg@pku.edu.cn*
[b]*College of Chemistry and Molecular Engineering, Peking University, Beijing, 100871, China*

† Electronic supplementary information (ESI) available. See DOI: 10.1039/c1jm11441g

graphene was transferred by the stamp method with the help of PMMA (poly methyl methacrylate)[26] to Si/300 nm SiO_2 substrates for Raman spectroscopy and electrical property characterization, to quartz substrates for transparency characterization, and to carbon-coated grids for high-resolution transmission electron microscopy (HRTEM) (Tecnai F30). Their electrical properties were measured by a Hall-effect measurement system (Accent HL5500).

The fabrication processes of a GNR/SNW heterojunction LED are as follows (Fig. 1): First, the as-synthesized large-scale graphene was transferred by the stamp method with the help of PMMA[26] to a Si/SiO_2 substrate. Second, the SNWs (ZnO, CdS, or CdSe) dispersed in ethanol were dropped on the substrate (Fig. 1a). Third, a photoresist pad was patterned to cover one end of a SNW by UV lithography and development processes (Fig. 1b). The photoresist together with the uncovered SNW was then used as the masks for the following graphene etching process by an inductively coupled plasma (ICP) etching technique (Fig. 1c). Later, the photoresist was removed by acetone, leaving a graphene pad connecting with a GNR underneath the SNW. Ohmic contact electrodes to the SNW (In/Au (10/100 nm)) and graphene pad (Au (60 nm)) were defined by UV lithography followed by a thermal evaporation and lift-off processes (Fig. 1d). It is worth noting that because an undercut was formed during the oxygen plasma etching process[21] (see ESI†), the In/Au electrode on the SNW will not make contact with the GNR and cause a short circuit. The electrical properties of the GNRs fabricated with the method mentioned above were investigated by measuring their transistor characteristics. The GNR transistor was fabricated by using a SiO_2 NW as the mask. Here, the insulative SiO_2 NW need not be removed before the electrical measurement, and thus avoids additional chemical or physical process induced influence to the measured results. The contact resistance to GNR was estimated by the four-terminal measurement method (see ESI†).

Room-temperature electrical transport properties of the GNR transistors and GNR/SNW heterojunctions were characterized with a semiconductor characterization system (Keithley 4200). The transparency was measured by a UV-vis-NIR recording spectrophotometer (Shimadzu UV-3100). Raman and EL measurements were done with a microzone confocal Raman spectroscope (HORIBA Jobin Yvon, LabRam HR 800) equipped with a color charge-coupled device (CCD).

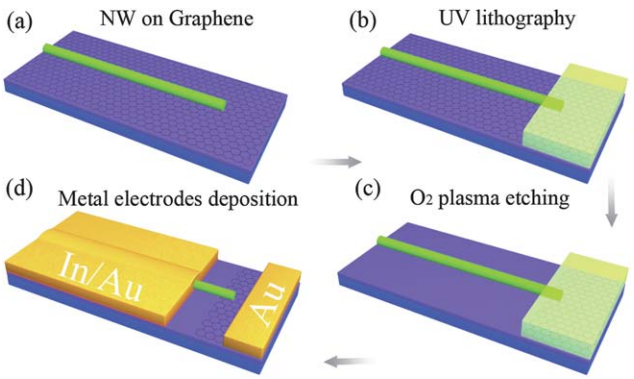

Fig. 1 Schematic illustration of the fabrication processes of a GNR/SNW heterojunction LED. (a) The as-synthesized large-scale graphene was transferred to a Si/SiO_2 substrate. After that, SNW suspension was dropped onto the graphene. (b) A photoresist pad was patterned to cover one end of a SNW by a UV lithography and development process. (c) Oxygen plasma etching was used to remove the exposed graphene. (d) After removing the photoresist, In/Au and Au ohmic contact electrodes attached to the SNW and graphene were defined, respectively.

Results and discussion

The HRTEM, Raman, and transparency characterization results for the as-synthesized graphenes (see ESI†) demonstrate that the graphene is high quality, a monolayer, with high transparency. The typical sheet resistance, hole concentration, and hole mobility of the graphenes, measured by a Hall measurement system, are about 345 Ω/sq, 1.84×10^{14} cm^{-2}, and 98.6 cm^2 V^{-1} s^{-1}, respectively. It is worth noting that the low sheet resistance and high hole concentration of the as-synthesized graphene guarantee a small series resistance in the heterojunction LED.

Fig. 2a shows a field-emission scanning electron microscope (FESEM) image of an as-fabricated GNR/CdS NW heterojunction LED. We can see that the diameter of the CdS NW is about 300 nm. During the electrical measurement, the In/Au ohmic contact electrode of the CdS NW was grounded. The *I–V* curve (Fig. 2b) of the LED shows an excellent rectification characteristic. An on/off current ratio of $\sim 3.4 \times 10^7$ can be obtained when the voltage changes from +1.5 to −1.5 V. The turn-on voltage is around 1.1 V. In view of the high hole concentration (1.84×10^{14} cm^{-2}) and near-zero band-gap of the GNR,[27] the heterojunction structure of the GNR/CdS NW LED can be considered approximately as a metal–semiconductor contact of the Schottky model.[28,29] For Schottky barrier diodes

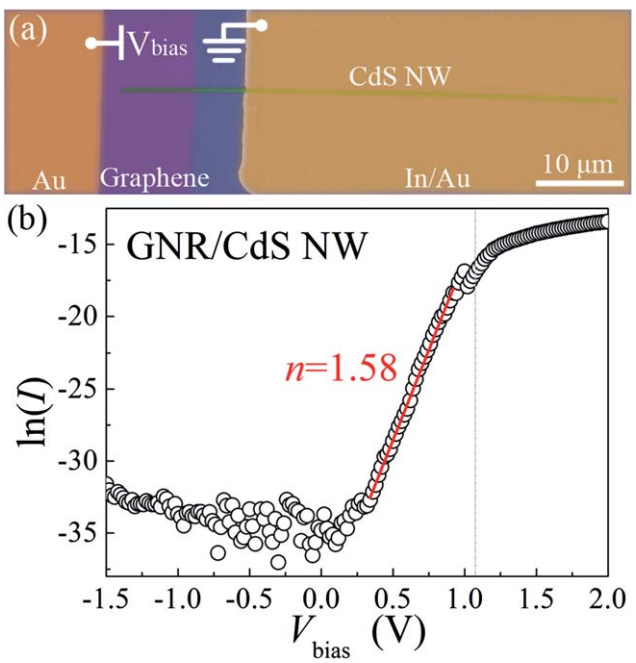

Fig. 2 (a) FESEM image of an as-fabricated GNR/CdS NW heterojunction LED. (b) Room-temperature *I–V* characteristic of the LED in panel (a) on a semi-log scale. The red straight line shows the fitting result of the *I–V* curve by the equation $\ln(I) = eV/nkT + \ln(I_0)$.

made on high-mobility semiconductors such as ZnO, CdS and CdSe *etc.*, the current I is determined by the thermionic emission of electrons and can be described by the equation $I = I_0[\exp(eV/nkT) - 1]$,[30] where I_0 is the reverse saturation current, e is the electronic charge, V is the applied bias, n is the diode ideality factor, k is the Bolzmann constant, and T is the absolute temperature. By fitting the measured I–V curve with the above equation, we can obtain $n = 1.58$. Note that, the GNR/ZnO NW and GNR/CdSe NW heterojunctions show similar rectification characteristics as above, with the turn-on voltages to be about 0.7 and 1.2 V, respectively (see ESI†).

Fig. 3a–c show the EL images (Olympus BX51M) of the GNR/SNW (ZnO, CdS, CdSe, respectively) heterojunction LEDs at a forward bias of 5 V. Except for the ZnO NW case (where the emitting light is invisible ultraviolet light) in Fig. 3a, strong emitting light spots can be seen clearly with naked eyes at the exposed ends of the NWs. For the CdS NW case (Fig. 3b), we can see another glaring light spot on the NW. This may be due to the scattering from defects or adhered particles on the CdS NW.[31] As the optical image of the graphene on the Si substrate with a 600 nm SiO_2 layer is unclear, we use the dashed lines to demarcate the graphene in these figures. Fig. 3d–f show the room-temperature normalized EL spectra at various forward biases for the GNR/SNW heterojunction LEDs, where the SNWs are ZnO, CdS, and CdSe NWs, respectively. The EL light collecting points were at the corresponding exposed ends of the NWs, indicated by the white arrows in the figures. The peak wavelengths of the EL spectra coincide with the band-edge emission of the involved SNWs (ZnO, CdS, CdSe, respectively.). This indicates the radiative recombination of electrons and holes occurs in the SNWs. For all the LEDs, EL intensities increase with the forward bias. Significantly, light emission can be detected at a forward bias as low as 2.5 V for the CdS NW case. We have studied more than 40 GNR/SNW heterojunction LEDs. Similar results are obtained.

We can qualitatively understand the mechanism of light emission for the GNR/SNW heterojunction LEDs by studying the energy band diagrams. Fig. 4a shows the thermal equilibrium energy band diagram of a graphene/n-type semiconductor structure, where the work function of graphene is Φ, and the electron affinity of the semiconductor is χ. E_g, E_F correspond to the band-gap and Fermi level of the semiconductor. Due to the difference of their work functions, the energy band of the semiconductor will bend upward at the graphene/semiconductor interface, and the Fermi levels at the two sides are brought into same level after contact. Under a forward bias (*i.e.*. a positive bias on graphene), the built-in potential is lowered. Therefore, more electrons will flow from the n-type semiconductor to graphene, and simultaneously, more holes will flow from the graphene to the n-type semiconductor. Herein, as the SNW is the direct band-gap semiconductor, which has a higher electron–hole radiative recombination rate, the injected holes and electrons will mainly recombine in the SNW region. Therefore, the corresponding EL spectrum will be determined by the band-edge emission of the SNW.

It is worth noting that, in our face-to-face contact LED, the active region, where the radiative recombination occurs, is larger and the series resistance is smaller, compared to crossed NW or NW/Si pad heterojunction structures.[22,32,33] In order to verify this, graphene pad/n-CdS NW heterojunction LEDs were also fabricated and studied for comparison. (see ESI†). These merits may benefit high-efficiency EL, and even electrically driven lasers in the future. More work aimed at further improving the device

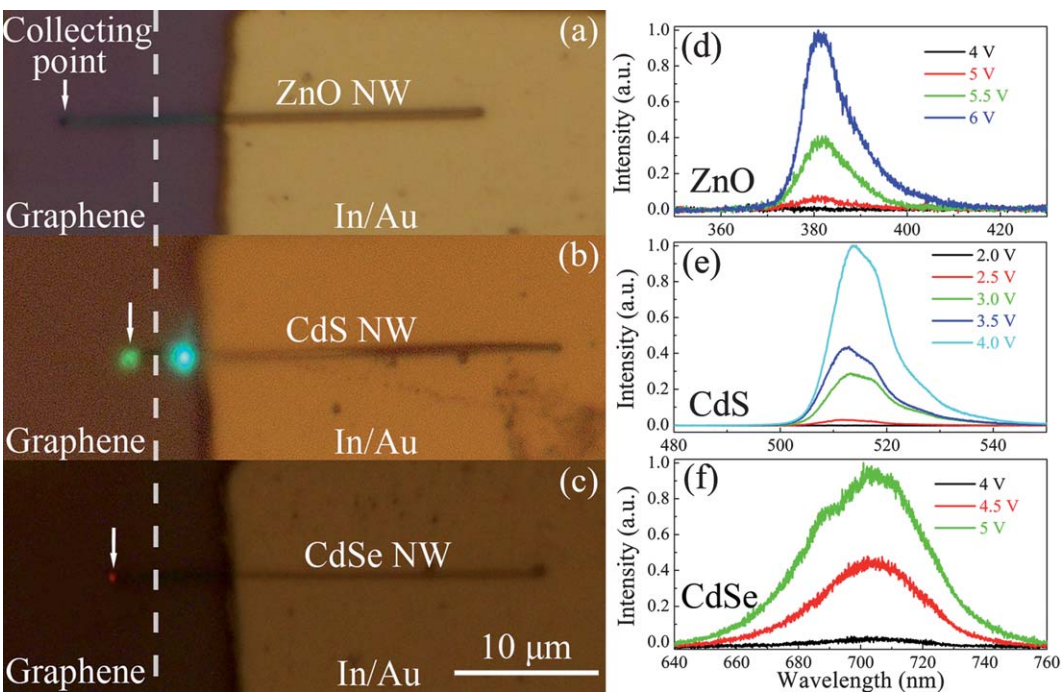

Fig. 3 (a)–(c) The optical images of the GNR/SNW (ZnO, CdS, CdSe, respectively) heterojunction LEDs at a forward bias of 5 V. Dashed lines were used to demarcate the graphene from the substrate. White arrows: the light collecting points during the EL measurements. (d)–(f) The room-temperature EL spectra for GNR/SNW (ZnO, CdS, CdSe, respectively) heterojunction LEDs at various forward biases.

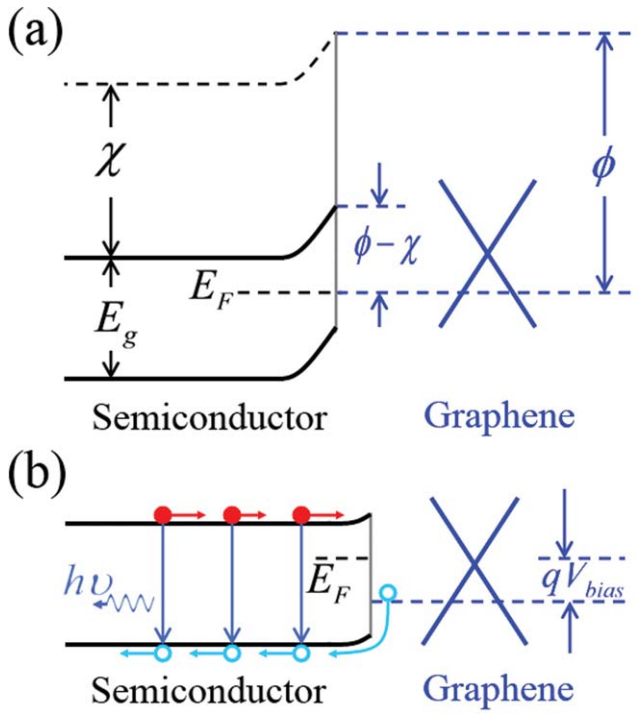

Fig. 4 Schematic illustration of the energy band diagram of a graphene/semiconductor heterojunction. (a) The thermal equilibrium energy band diagram. (b) The energy band diagram of the heterojunction under a forward bias. Φ: the work function of graphene; χ: the electron affinity of the semiconductor.

performance, including optimizing the SNWs, graphene materials, device structure, as well as the fabrication process, is still ongoing in our lab.

Conclusion

We have fabricated and studied GNR/SNW heterojunction LEDs for the first time. In the device, the GNR and SNW have a face-to-face contact structure, which has the merits of a larger active region and smaller series resistance. ZnO, CdS, and CdSe NWs were employed in our case. The emitting light wavelengths of the as-fabricated LEDs are determined by the band-gaps of the involved SNWs, which can vary from ultraviolet (380 nm) to green (513 nm) to red (705 nm). Our work opens new routes to developing diverse graphene-based nano-optoelectronic devices, which are basic components in integrated optoelectronic systems. Besides, the novel graphene/SNW hybrid devices, by taking advantage of both graphene and SNWs, have promise for use in applications such as high-sensitivity sensor and transparent flexible devices in the future.

Acknowledgements

This work was supported by the National Natural Science Foundation of China (No. 10774007, 11074006, 10874011, 50732001), the National Basic Research Program of China (No. 2007CB613402), and the Fundamental Research Funds for the Central Universities.

References

1 K. S. Novoselov, A. K. Geim, S. V. Morozov, D. Jiang, Y. Zhang, S. V. Dubonos, I. V. Grigorieva and A. A. Firsov, *Science*, 2004, **306**, 666–669.
2 Y. M. Lin, K. A. Jenkins, A. Valdes-Garcia, J. P. Small, D. B. Farmer and P. Avouris, *Nano Lett.*, 2009, **9**, 422–426.
3 K. S. Novoselov, Z. Jiang, Y. Zhang, S. V. Morozov, H. L. Stormer, U. Zeitler, J. C. Maan, G. S. Boebinger, P. Kim and A. K. Geim, *Science*, 2007, **315**, 1379.
4 F. Bonaccorso, Z. Sun, T. Hasan and A. C. Ferrari, *Nat. Photonics*, 2010, **4**, 611–622.
5 A. K. Geim and K. S. Novoselov, *Nat. Mater.*, 2007, **6**, 183–191.
6 K. I. Bolotin, K. J. Sikes, Z. Jiang, M. Klima, G. Fudenberg, J. Hone, P. Kim and H. L. Stormer, *Solid State Commun.*, 2008, **146**, 351–355.
7 X. S. Li, Y. W. Zhu, W. W. Cai, M. Borysiak, B. Y. Han, D. Chen, R. D. Piner, L. Colombo and R. S. Ruoff, *Nano Lett.*, 2009, **9**, 4359–4363.
8 C. Lee, X. D. Wei, J. W. Kysar and J. Hone, *Science*, 2008, **321**, 385–388.
9 B. D. Briggs, B. Nagabhirava, G. Rao, R. Geer, H. Y. Gao, Y. Xu and B. Yu, *Appl. Phys. Lett.*, 2010, **97**, 223102.
10 L. G. de Arco, Y. Zhang, C. W. Schlenker, K. Ryu, M. E. Thompson and C. W. Zhou, *ACS Nano*, 2010, **4**, 2865–2873.
11 J. B. Wu, M. Agrawal, H. A. Becerril, Z. N. Bao, Z. F. Liu, Y. S. Chen and P. Peumans, *ACS Nano*, 2010, **4**, 43–48.
12 K. S. Kim, Y. Zhao, H. Jang, S. Y. Lee, J. M. Kim, K. S. Kim, J. H. Ahn, P. Kim, J. Y. Choi and B. H. Hong, *Nature*, 2009, **457**, 706–710.
13 Y. Zheng, G. X. Ni, C. T. Toh, M. G. Zeng, S. T. Chen, K. Yao and B. Özyilmaz, *Appl. Phys. Lett.*, 2009, **94**, 163505.
14 Y. Zhou and K. P. Loh, *Adv. Mater.*, 2010, **22**, 3615–3620.
15 C. Berger, Z. M. Song, T. B. Li, X. B. Li, A. Y. Ogbazghi, R. Feng, Z. T. Dai, A. N. Marchenkov, E. H. Conrad, P. N. First and W. A. de Heer, *J. Phys. Chem. B*, 2004, **108**, 19912–19916.
16 C. Berger, Z. M. Song, X. B. Li, X. S. Wu, N. Brown, C. Naud, D. Mayou, T. B. Li, J. Hass, A. N. Marchenkov, E. H. Conrad, P. N. First and W. A. de Heer, *Science*, 2006, **312**, 1191–1196.
17 J. M. Lee, J. W. Choung, J. Yi, D. H. Lee, M. Samal, D. K. Yi, C. H. Lee, G. C. Yi, U. Paik, J. A. Rogers and W. I. Park, *Nano Lett.*, 2010, **10**, 2783–2788.
18 P. D. Yang, R. X. Yan and M. Fardy, *Nano Lett.*, 2010, **10**, 1529–1536.
19 S. Ju, A. Facchetti, Y. Xuan, J. Liu, F. Ishikawa, P. D. Ye, C. W. Zhou, T. J. Marks and D. B. Janes, *Nat. Nanotechnol.*, 2007, **2**, 378–384.
20 B. Z. Tian, T. Cohen-Karni, Q. Qing, X. J. Duan, P. Xie and C. M. Lieber, *Science*, 2010, **329**, 830–834.
21 C. Liu, L. Dai, Y. Ye, T. Sun, R. M. Peng, X. N. Wen, P. C. Wu and G. G. Qin, *J. Mater. Chem.*, 2010, **20**, 5011–5015.
22 W. Q. Yang, H. B. Huo, L. Dai, R. M. Ma, S. F. Liu, G. Z. Ran, B. Shen, C. L. Lin and G. G. Qin, *Nanotechnology*, 2006, **17**, 4868–4872.
23 Y. Ye, L. Dai, X. N. Wen, P. C. Wu, R. M. Pen and G. G. Qin, *ACS Appl. Mater. Interfaces*, 2010, **2**, 2724–2727.
24 C. Liu, P. C. Wu, T. Sun, L. Dai, Y. Ye, R. M. Ma and G. G. Qin, *J. Phys. Chem. C*, 2009, **113**, 14478–14481.
25 Y. Ye, L. Gan, L. Dai, X. F. Guo, H. Meng, B. Yu, Z. J. Shi, K. P. Shang and G. G. Qin, *Nanoscale*, 2011, **3**, 1477–1481.
26 A. Reina, X. T. Jia, J. Ho, D. Nezich, H. Son, V. Bulovic, M. S. Dresselhaus and J. Kong, *Nano Lett.*, 2009, **9**, 30–35.
27 A. H. Castro Neto, F. Guinea, N. M. R. Peres, K. S. Novoselov and A. K. Geim, *Rev. Mod. Phys.*, 2009, **81**, 109–162.
28 D. Thomas, J. Boettcher, M. Burghard and K. Kern, *Small*, 2010, **6**, 1868–1872.
29 X. M. Li, H. W. Zhu, K. L. Wang, A. Y. Cao, J. Q. Wei, C. Y. Li, Y. Jia, Z. Li, X. Li and D. H. Wu, *Adv. Mater.*, 2010, **22**, 2743–2748.
30 B. L. Sharma, *Metal-Semiconductor Schottky Barrier Junctions and Their Applications*; Plenum Press: New York, 1984.
31 R. M. Ma, X. L. Wei, L. Dai, S. F. Liu, T. Chen, S. Yue, Z. Li, Q. Chen and G. G. Qin, *Nano Lett.*, 2009, **9**, 2679–2703.
32 Z. H. Zhong, F. Qian, D. L. Wang and C. M. Lieber, *Nano Lett.*, 2003, **3**, 343–346.
33 M. S. Gudiksen, L. J. Lauhon, J. F. Wang, D. C. Smith and C. M. Lieber, *Nature*, 2002, **415**, 617–620.